ARTICLE IN PRESS

European Journal of Control xxx (xxxx) xxx

Contents lists available at ScienceDirect

European Journal of Control

journal homepage: www.sciencedirect.com/journal/european-journal-of-control

Optimal trajectory planning for anti-sloshing motion control

Francesco Grassi [a], Gianni Bianchini [b,*], Simone Paoletti [b], Tommaso Matassini [a]

[a] Marchesini Group S.p.A., Div. CO.RI.M.A., Strada delle Frigge 15, Monteriggioni, Siena, 53035, Italy
[b] Dipartimento di Ingegneria dell'Informazione e Scienze Matematiche, Universitá di Siena, Via Roma 56, 53100, Siena, Italy

ARTICLE INFO

Recommended by T Parisini

Keywords:
Anti-sloshing motion control
Trajectory planning
Optimal control

ABSTRACT

The phenomenon of sloshing, i.e., the oscillation of liquids inside partially filled containers during motion, represents a significant challenge in transportation and process engineering. This paper addresses the design of an optimized motion law to reduce unwanted liquid oscillations in automated liquid handling processes. A constrained optimization problem based on a linearized sloshing model is designed with the aim of minimizing liquid oscillation both during movement and in the subsequent resting phase. To experimentally validate the proposed method, a dedicated experimental setup is designed, including a controlled motion system and a visual tracking system. Experimental tests confirm the reliability of the optimized motion law.

1. Introduction

Sloshing, i.e., the uncontrolled vibration of the free surface of a liquid, is intrinsic to the motion of a partially filled container. Due to the demanding motion requirements of recent liquid packaging machines, oscillations of the free surface may cause overflows or unwanted soiling of the containers, thus calling for ad-hoc anti-sloshing trajectory planning. To this purpose, in Richter (2010) a sliding-mode approach is designed, but its application is limited by the requirement of real-time measurement of the sloshing height. In the specific context of packaging industry, trajectory planning is formulated in Grundelius and Bernhardsson (1999) as a minimum-energy optimization problem, whereas Grundelius (2000) employs an iterative learning control strategy based on experimental measurements of the liquid state. The latter approaches consider the rectangular container case and are numerical in nature and computationally demanding. The work in Di Leva et al. (2021) formulates an optimization problem to generate time-optimal spatial trajectories parameterized as B-splines. In Yano and Terashima (2005), a hybrid-shape strategy combining notch and low-pass filters is proposed for three-dimensional paths, while Noda et al. (2004) devise a similar technique exploiting the effect of controlled container tilting. Nevertheless, tilting-based approaches are unsuitable when the container orientation must remain fixed, as it is commonly required in packaging operations. Another class of anti-sloshing trajectory design methods relies on optimization techniques for linear dynamic systems. Among these, input shaping based on a specific class of Finite Impulse Response (FIR) filters has been investigated. This approach has been employed to mitigate sloshing in cylindrical containers transported by robotic manipulators in Aribowo et al. (2015). Robust shapers are validated using rectangular containers in Pridgen et al. (2010), while more complex configurations such as pendulum-suspended containers are addressed in Alshaya and Almujarrab (2021), Khorshid and Al-Fadhli (2020). Although input shaping remains the predominant strategy, alternative formulations have been proposed, including anti-sloshing trajectory generation using Infinite Impulse Response (IIR) filters in Feddema et al. (1997), or FIR exponential filters in Melchiorri et al. (2018). To the best of the authors' knowledge, all the above techniques have been validated only under relatively low-bandwidth conditions, with maximum container accelerations on the order of $2.5\,\mathrm{m\,s^{-2}}$. In contrast, automatic packaging machinery requires trajectories with predefined durations to ensure synchronization with concurrent product-handling operations, leading to considerably higher acceleration levels.

In the recent work (Guagliumi et al., 2021) a simple methodology is exploited to predict the sloshing height for containers following prescribed planar trajectories. Such method employs a linear mass-spring-damper model to describe the sloshing dynamics, and has been experimentally proved to accurately estimate the maximum free-surface elevation even under highly dynamic motion conditions. Using the above model, Guagliumi et al. (2022) develop a technique for fast rest-to-rest rectilinear motions, aimed at both controlling the maximum sloshing height during movement and the residual oscillation of the liquid after the motion ends. Indeed, intermittent rectilinear motions represent the most common case in packaging machines, where a rest period is in place between successive translations. In such applications, the maximum sloshing height during motion must be kept below a given threshold to prevent overflows or contamination of the container walls, while

* Corresponding author.
E-mail addresses: francesco.grassi@marchesini.com (F. Grassi), giannibi@diism.unisi.it (G. Bianchini), paoletti@diism.unisi.it (S. Paoletti), tommaso.matassini@marchesini.com (T. Matassini).

https://doi.org/10.1016/j.ejcon.2026.101613
Received 18 June 2026; Accepted 22 July 2026
Available online 25 July 2026

Please cite this article as: Francesco Grassi et al., *European Journal of Control,* https://doi.org/10.1016/j.ejcon.2026.101613

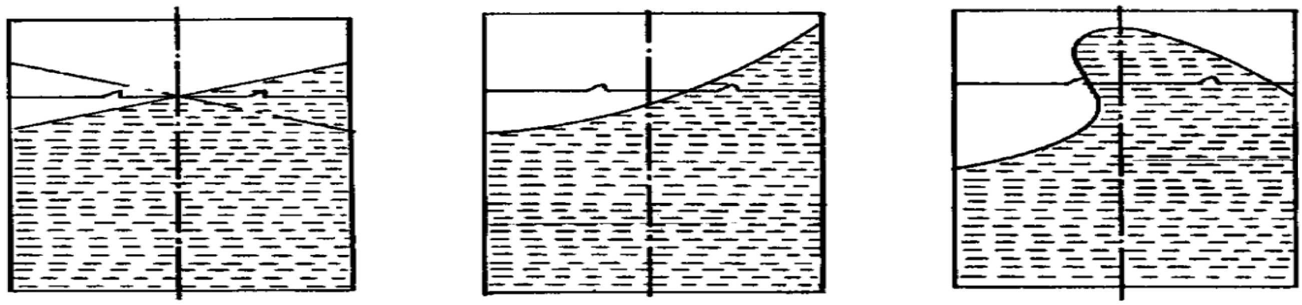

(a) Linear motion regime. (b) Weakly nonlinear motion regime. (c) Highly nonlinear motion regime.

Fig. 1. Schematic representation of possible liquid motion regimes (Ibrahim, 2005).

residual oscillations after the motion ends must be quickly suppressed in order to ensure predictable conditions for subsequent operations (e.g., weighing).

1.1. Paper contribution

This paper focuses on optimal design of rectilinear motion trajectories aimed at mitigating the sloshing phenomenon. As opposed to the methodology in Guagliumi et al. (2022), which is based on the optimization of the parameters of predefined well-established motion laws such as polynomial and trapezoidal ones (see Biagiotti & Melchiorri, 2008), in this work the sampled motion trajectory is optimized directly by solving a fixed-horizon constrained optimal control problem. This allows for generating a reference trajectory which spans a prescribed time interval and satisfies both a maximum sloshing height constraint and suitable boundary conditions on acceleration and jerk in order to ensure low residual oscillation when the motion ends. The considered performance functional is LQR-like in order to trade off regulation performance and control effort. The obtained optimal trajectory is then tracked on the motion system using a high-bandwidth low-level controller as in previous approaches, thus not requiring feedback from liquid level measurements.

Experimental validation is conducted on a dedicated testbed consisting of a motion system and a vision-based measurement system to monitor liquid oscillations. Experimental results are compared to those obtained via the technique in Guagliumi et al. (2022), showing a significant reduction in liquid oscillation both during motion and in the subsequent resting phase.

The paper is organized as follows: in Section 2, the employed sloshing model is recalled, the proposed trajectory planning technique is developed in Section 3, the experimental validation is presented and discussed in Section 4, and conclusions are finally drawn in Section 5.

2. Modeling the sloshing phenomenon

We consider the sloshing phenomenon in a cylindrical container partially filled with liquid and subject to 1-D straight motions. To describe this phenomenon, three distinct dynamic regimes can be identified for the motion of the liquid free surface (Ibrahim, 2005):

- **Linear motion regime**: The free surface remains planar (Fig. 1a), oscillating around a fixed nodal diameter perpendicular to the excitation plane. This regime occurs for small oscillations induced by limited accelerations of the container.
- **Weakly nonlinear motion regime**: The free surface becomes curved (Fig. 1b) and rotary sloshing emerges with the nodal diameter rotating around the container axis. This regime occurs for oscillations with greater amplitude and closer to resonance frequencies.
- **Highly nonlinear motion regime**: Abrupt velocity changes in the free surface create discontinuities, resulting in liquid impacts on the container walls and pressure spikes (Fig. 1c).

To the purpose of the control problem addressed in this paper, the linear motion regime is considered. The sloshing phenomenon is described through an equivalent mechanical model represented by a linear mass-spring-damper model. For the equivalent mechanical model of the weakly nonlinear motion regime, the interested reader is referred to Bauer (1966). In the following, all quantities are expressed in SI units, unless otherwise noted.

2.1. Linear sloshing model

The linear equivalent mechanical model is borrowed from Guagliumi et al. (2021). It considers a cylindrical container of radius R, filled with a liquid of density ρ and height h. The sloshing phenomenon is approximated by a single oscillating mass m, connected to the container by a spring with stiffness k and a damper with damping constant c, as shown in Fig. 2.

Assuming that the container moves only along the horizontal axis of a fixed reference frame with origin O, let x_0 be the absolute position of the vertical axis of the cylinder and x be the horizontal displacement of the mass m relative to the container's reference frame, having the origin O' on the vertical axis of the cylinder. The motion of the mass m is then described by the Second Newton's Law as follows:

$$m\left(\ddot{x} + \ddot{x}_0\right) = -k\,x - c\,\dot{x}, \tag{1}$$

which can be rewritten as:

$$\ddot{x} + 2\zeta\omega_n\dot{x} + \omega_n^2 x = -\ddot{x}_0, \tag{2}$$

with $\omega_n = \sqrt{k/m}$ the natural frequency and $\zeta = c/(2\sqrt{km})$ the damping ratio of the fundamental sloshing mode.

Remark 1. The linear model in Guagliumi et al. (2021) includes several moving masses, each representing the equivalent mass of a sloshing mode. In this paper we consider only the fundamental mode, motivated by the observation that it dominates the liquid motion, carrying most of the system energy. Higher-order modes have higher frequencies and are more significantly damped, contributing less to the overall liquid oscillations.

Expressions for the natural frequency ω_n and the damping ratio ζ to be used in (2) for the fundamental mode can be found in Guagliumi et al. (2021). In particular, the expression for ω_n^2 looks as follows:

$$\omega_n^2 = \frac{g\,\xi_1}{R}\tanh\left(\frac{\xi_1\,h}{R}\right), \tag{3}$$

where g is the gravitational acceleration and ξ_1 is a known constant adimensional parameter, whose value is tabulated (see Guagliumi et al., 2021). Notice the dependence of ω_n on the liquid height h.

2.2. Sloshing height

The sloshing mass position x in (2) is an abstract quantity that lacks direct physical meaning, as it represents the displacement of an

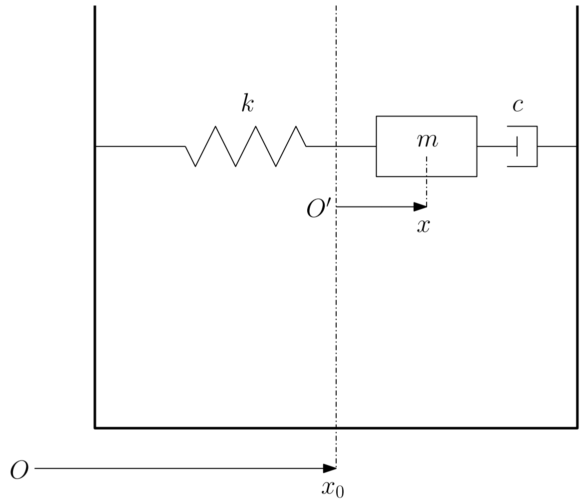

Fig. 2. Scheme of the equivalent linear mechanical model considering only the sloshing mass of the fundamental mode.

equivalent oscillating mass rather than the actual motion of the liquid surface. However, the sloshing mass position can be used to reconstruct the sloshing height relative to the undisturbed liquid surface, which occurs at the container edge along the plane of excitation.

The expression for the sloshing height $\overline{\eta}$ as a function of the sloshing mass position x is derived in Guagliumi et al. (2021), assuming the free liquid surface to be planar, as shown in Fig. 3. It is given by:

$$\overline{\eta} = \frac{4m}{\pi R^3 \rho}\, x. \tag{4}$$

The formula holds under small oscillations, where nonlinear effects such as wave breaking or asymmetric deformations of the free surface are negligible.

3. Optimal anti-sloshing trajectory design

The term $\ddot{x}_0$ in (2) is the container acceleration, causing the displacement x of the mass m and consequently the sloshing effect, see (4). The problem addressed in this paper is to design $\ddot{x}_0$ with the aim of minimizing the peak sloshing height along the container motion, while reducing residual oscillations when the container stops. To this aim, we propose to optimize the motion law by solving a fixed-horizon constrained optimal control problem.

3.1. Linear state-space models

Let the state vector at time t be defined as:

$$\Psi(t) = [\, x_0(t),\ \dot{x}_0(t),\ \ddot{x}_0(t),\ x(t),\ \dot{x}(t)\,]', \tag{5}$$

and consider the jerk of the container as the system input $u(t)$, namely:

$$u(t) = \dddot{x}_0(t). \tag{6}$$

The dynamics of $\Psi(t)$ is described by the continuous-time linear time-invariant state-space model:

$$\dot{\Psi}(t) = A\Psi(t) + Bu(t), \tag{7}$$

where the matrices A and B are defined as:

$$A = \begin{bmatrix} 0 & 1 & 0 & 0 & 0 \\ 0 & 0 & 1 & 0 & 0 \\ 0 & 0 & 0 & 0 & 0 \\ 0 & 0 & 0 & 0 & 1 \\ 0 & 0 & -1 & -\omega_n^2 & -2\zeta_n\omega_n \end{bmatrix}, \quad B = \begin{bmatrix} 0 \\ 0 \\ 1 \\ 0 \\ 0 \end{bmatrix}. \tag{8}$$

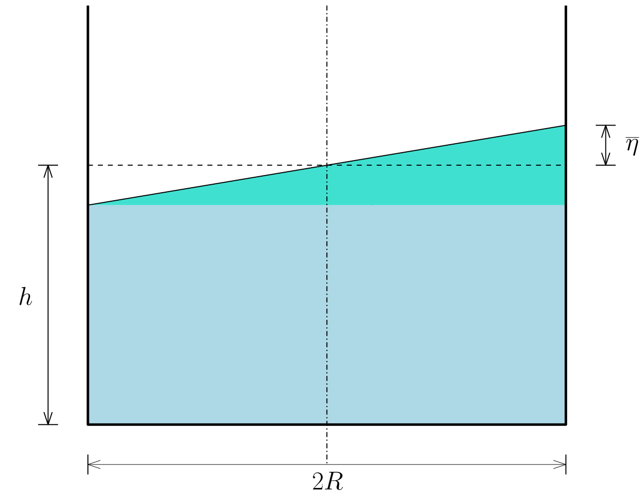

Fig. 3. Scheme of the sloshing height model assuming planar free liquid surface.

Remark 2. One could have used the acceleration of the container as the system input. However, considering the jerk leaves flexibility for bounding it in the optimization problem to avoid undesired vibrations due to excessively high jerk values.

Assuming a zero-order hold, the continuous-time model (7) is discretized exactly using standard formulas. Let T be the sampling period, defined as:

$$T = \frac{t_{motion}}{N}, \tag{9}$$

where t_{motion} is the total motion duration and N is the number of discrete steps into which t_{motion} is divided. Moreover, let the sampled state vector be $\widetilde{\Psi}(k) = \Psi(kT)$, and the sampled input be $\widetilde{u}(k) = u(kT)$, where $k = 0, 1, 2, \ldots$ is the discrete time index. The dynamics of $\widetilde{\Psi}(k)$ is described by the discrete-time linear time-invariant state-space model:

$$\widetilde{\Psi}(k+1) = A_d\, \widetilde{\Psi}(k) + B_d\, \widetilde{u}(k), \tag{10}$$

where the matrices A_d and B_d are given by:

$$A_d = e^{AT}, \quad B_d = \int_0^T e^{A\tau} B\, d\tau. \tag{11}$$

3.2. Optimal control problem

We formulate a regulation problem where the objective is to drive the system state to zero from an initial condition $\widetilde{\Psi}(0)$. This is achieved by minimizing a quadratic cost function, while satisfying linear constraints on both the control input and the system states (Rawlings et al., 2022). The resulting problem is a linearly constrained quadratic program that can be solved using state-of-the-art solvers.

The cost function to be minimized is defined as:

$$J = \sum_{k=0}^{N-1} \widetilde{\Psi}(k)'\, Q\, \widetilde{\Psi}(k) + \widetilde{u}(k)'\, R\, \widetilde{u}(k), \tag{12}$$

where Q and R are symmetric, positive definite weighting matrices for the states and the control inputs, respectively.

Regarding the constraints, these include the state dynamics (10) for $k = 0, 1, \ldots, N-1$. In addition, the following constraints are considered.

3.2.1. Output constraints

Let $\overline{\eta}_{\max} > 0$ be the maximum tolerated sloshing height. Using (4), the constraint $|\overline{\eta}| \le \overline{\eta}_{\max}$ can be translated into a constraint on the displacement x, namely:

$$|x| \le \frac{\overline{\eta}_{max} \pi R^3 \rho}{4m} \triangleq x_{max}. \tag{13}$$

Recalling that x is the fourth entry of the state vector Ψ, the latter constraint can be rewritten as:

$$F\,\widetilde{\Psi}(k) \leq f, \quad k = 0, 1, \ldots, N, \tag{14}$$

where:

$$F = \begin{bmatrix} 0 & 0 & 0 & 1 & 0 \\ 0 & 0 & 0 & -1 & 0 \end{bmatrix}, \quad f = \begin{bmatrix} x_{max} \\ x_{max} \end{bmatrix}. \tag{15}$$

3.2.2. Input constraints

A maximum jerk value $u_{\max}$ is imposed to avoid excessively high values, which could induce vibrations in the machine during container handling (see Remark 2). The corresponding constraint $|\widetilde{u}(k)| \leq u_{\max}$ is rewritten as:

$$E\,\widetilde{u}(k) \leq e, \quad k = 0, 1, \ldots, N-1, \tag{16}$$

where:

$$E = \begin{bmatrix} 1 \\ -1 \end{bmatrix}, \quad e = \begin{bmatrix} u_{max} \\ u_{max} \end{bmatrix}. \tag{17}$$

3.2.3. Initial state

The initial position of the container is set to $-s_0$, where s_0 represents the total distance to be covered during the motion. Since the system starts from rest, all other state entries are initially set to zero, including the acceleration of the container. This is done to enforce a smooth start of the motion, without undesired vibrations. The resulting initial state is:

$$\widetilde{\Psi}(0) = \Psi_0 \triangleq [\,-s_0,\ 0,\ 0,\ 0,\ 0\,]'. \tag{18}$$

3.2.4. Terminal state

The terminal value is set to zero for all the state entries:

$$\widetilde{\Psi}(N) = \mathbf{0} \triangleq [\,0,\ 0,\ 0,\ 0,\ 0\,]'. \tag{19}$$

This guarantees that the container stops in the right position at the end of the motion. Moreover, imposing that both position and velocity of the sloshing mass are zero at the final time step is expected to mitigate the residual oscillations of the liquid in the real system. This is also pursued by imposing that the container arrives at the final position with zero acceleration.

Summarizing, the formulated optimization problem looks as follows:

$$\begin{cases} \min_{\widetilde{\Psi},\widetilde{u}} & \sum_{k=0}^{N-1} \widetilde{\Psi}(k)'\,Q\,\widetilde{\Psi}(k) + \widetilde{u}(k)'\,R\,\widetilde{u}(k) \\ \text{s.t.} & \widetilde{\Psi}(k+1) = A_d\,\widetilde{\Psi}(k) + B_d\,\widetilde{u}(k) \\ & F\,\widetilde{\Psi}(k) \leq f \\ & E\,\widetilde{u}(k) \leq e, \quad k = 0, \ldots, N-1 \\ & \widetilde{\Psi}(0) = \Psi_0 \\ & \widetilde{\Psi}(N) = \mathbf{0}. \end{cases} \tag{20}$$

3.3. Control system structure

The solution of (20) provides the optimal state sequence $\widetilde{\Psi}(k)$, from which it is possible to extract the optimal profiles for x_0, $\dot{x}_0$ and $\ddot{x}_0$. Such profiles are supplied off-line as references to a low-level control system which controls the container motion accordingly (see Fig. 4). Notice that solving problem (20) also returns the optimal jerk sequence $\widetilde{u}(k)$, which is only instrumental and not directly implemented in the control system.

4. Experimental results

To experimentally validate the proposed method, a motion system has been used to accurately implement the optimized trajectories. This section describes the experimental setup that has been built and the results obtained with both the proposed and state-of-the-art approaches.

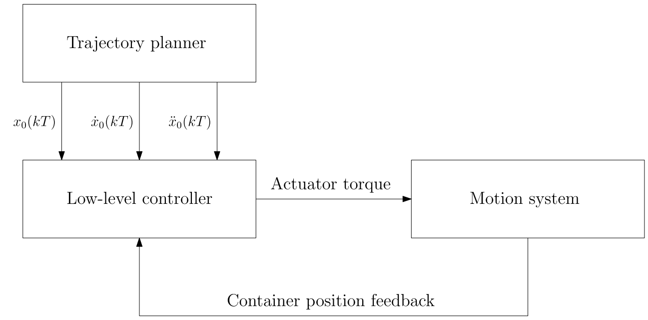

Fig. 4. Control system architecture. The trajectory profile $x_0(kT)$, $\dot{x}_0(kT)$, $\ddot{x}_0(kT)$ is fed off-line to the low-level controller.

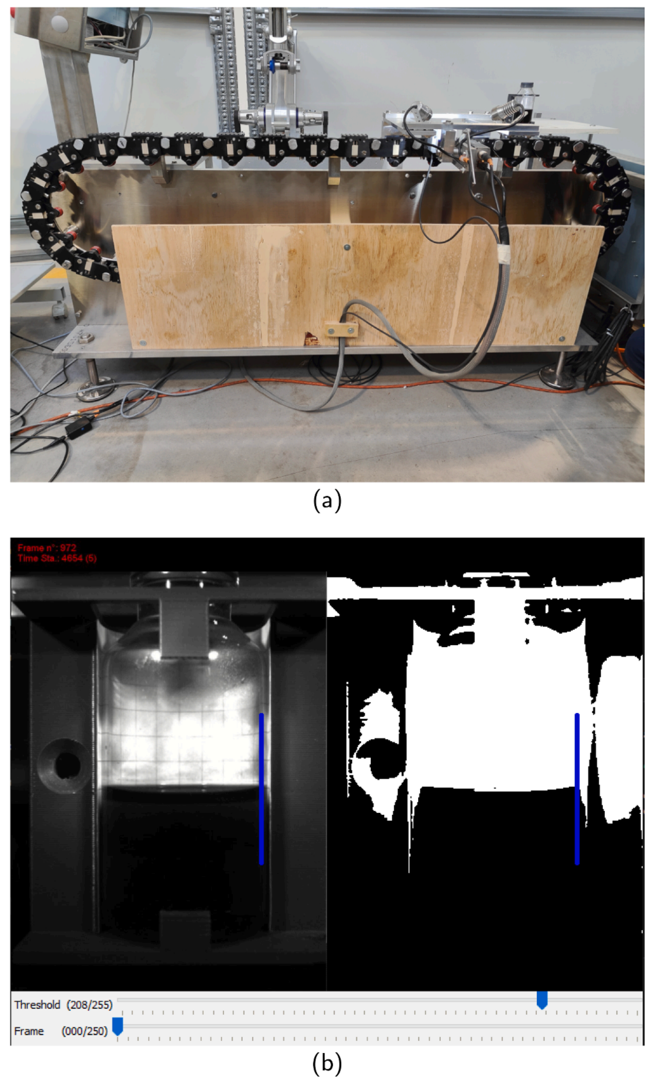

Fig. 5. (a) Experimental setup. (b) sloshing tracking system.

4.1. Experimental setup

The experimental setup consists of a Beckhoff brushless motor, coupled with a reduction gearbox and a pulley, which transmits motion to a transport belt via a timing belt (see Fig. 5(a)). The transport belt is composed of several sliding carriages, one of which is equipped with a custom-designed support to securely hold a vial during movement. The design of the bottle holder prevents any unintended displacements that could influence the liquid oscillations. In this way, the observed

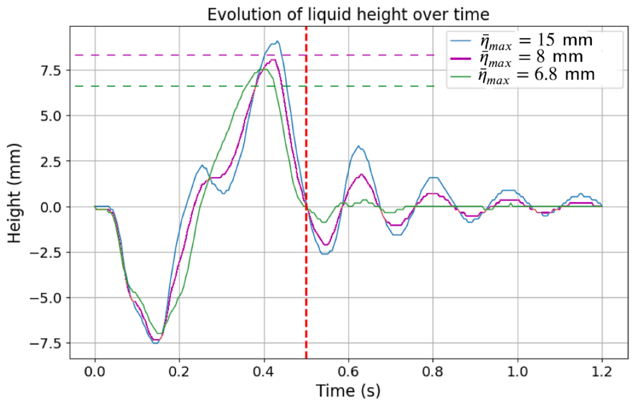

Fig. 6. Experimental sloshing height over time under three different maximum height constraints: $\bar{\eta}_{\max} = 15$ mm (solid blue), $\bar{\eta}_{\max} = 8$ mm (solid magenta), $\bar{\eta}_{\max} = 6.8$ mm (solid green). Dashed horizontal lines of the corresponding color represent the sloshing height constraints. The line corresponding to $\bar{\eta}_{\max} = 15$ mm is not shown in order to preserve picture readability. The vertical red dashed line separates the motion and resting phases.

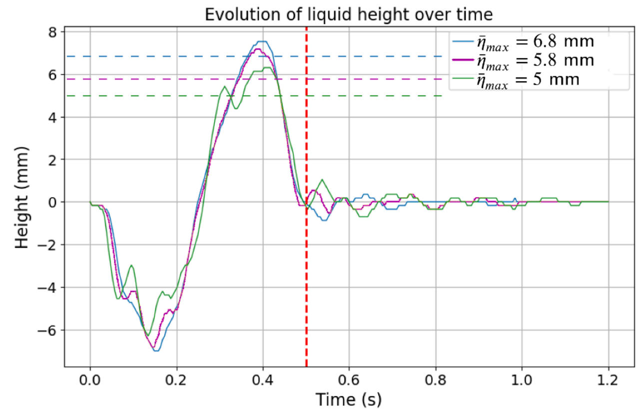

Fig. 7. Experimental sloshing height over time imposing stringent maximum sloshing height: $\bar{\eta}_{\max} = 6.8$ mm (solid blue), $\bar{\eta}_{\max} = 5.8$ mm (solid magenta), $\bar{\eta}_{\max} = 5$ mm (solid green). Dashed lines of the corresponding color represent the sloshing height constraints.

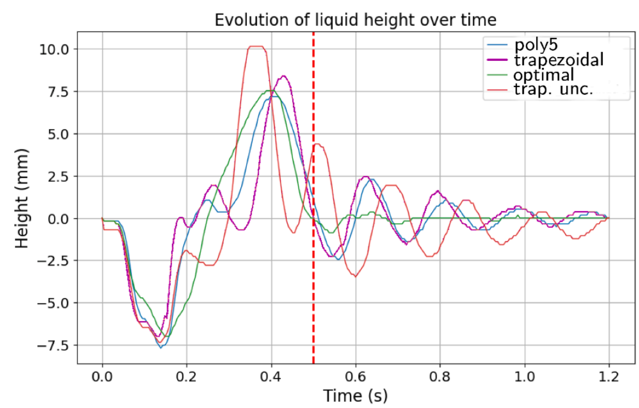

Fig. 8. Experimental sloshing height over time under different motion laws: the proposed *optimal* one, and the *poly5*, *trapezoidal*, and *trapezoidal with unconstrained velocity* trajectories from Biagiotti and Melchiorri (2008), Guagliumi et al. (2022).

fluctuations in the liquid level are exclusively due to the fluid dynamics. The experiments were conducted using a 10R-type vial, with radius $R = 13$ mm and filling height $h = 28$ mm. Single translation movements spanning $s_0 = 192$ mm with a total movement time of 1.2 s ($t_{motion} = 0.5$ s of forward motion and 0.7 s of rest phase) have been performed.

The motion system is controlled via a low-level high-bandwidth controller that precisely tracks the target trajectories given in the form of a sequence of points $(x_0, \dot{x}_0, \ddot{x}_0)$ sampled at 1 ms, with a position error below 0.3%. To capture experimental data, a Basler piA640-210gm camera is used, mounted on a support installed on two blocks adjacent to the bottle-holding block. This setup ensures that the camera continuously tracks the container throughout its movement. The captured images are then stored and later compiled into a 30fps video. The oscillation of the liquid at the right edge of the bottle is then evaluated from the video. This process involves creating a binary mask, highlighting in black the regions containing the liquid. As shown in Fig. 5 (b), a selected rectangular region near the right edge is analyzed to determine the highest black pixel, corresponding to the maximum liquid level. This pixel value is subsequently converted into millimeters and normalized with respect to the initial liquid height, providing a measurement of the height variation relative to the starting condition.

4.2. Results and discussion

In the following validation tests, matrices Q and R in the optimization problem have been chosen as the identity matrix. A comparison has been carried out between three runs of the optimized trajectories obtained via the proposed method for three different values of the design parameter $\bar{\eta}_{\max}$. Fig. 6 depicts the time evolution of the sloshing height for such trajectories. For $\bar{\eta}_{\max} = 15$ mm, it turns out that constraint (14) is never active, while it becomes a determining factor for the other two cases, i.e., $\bar{\eta}_{\max} = 8$ mm and $\bar{\eta}_{\max} = 6.8$ mm. It is apparent that progressively reducing the maximum height bound leads to an improvement during the motion phase but also in the resting phase. In particular, the residual oscillations of the liquid once the container has stopped are significantly reduced for lower $\bar{\eta}_{\max}$. Note that the measured peak height turns out to be slightly higher than $\bar{\eta}_{\max}$ in the most restrictive case, due to model errors. In all cases, the peak acceleration during the motion phase amounts to around $5\,\mathrm{m\,s^{-2}}$, which is considerably higher than that achieved by other design methodologies. It turns out that further reducing $\bar{\eta}_{\max}$ introduces undesirable effects. In particular, during the resting phase, the behavior slightly worsens due to vibrations in the handling system, caused by the high acceleration and jerk values imposed by the stricter constraint. The impact of vibrations is not limited to the resting phase but also affects the motion phase (see Fig. 7). To further demonstrate the performance of the proposed design, an experimental comparative analysis has been conducted against the optimized motion curves proposed in Biagiotti and Melchiorri (2008), Guagliumi et al. (2022), namely the optimized *poly5*, *trapezoidal*, and *trapezoidal with unconstrained velocity* trajectories, by designing their parameters according to the experimental testbed. The proposed *optimal* motion law is designed for $\bar{\eta}_{\max} = 6.7$ mm. In Fig. 8, the experimental time plots of the sloshing height under the various motion laws are compared.

A quantitative comparison of the peak sloshing heights under the different motion laws is reported in Table 1, where $\bar{\eta}_{peak}$ represents the maximum sloshing height recorded during the motion phase, $|\bar{\eta}_{rest,peak}|$ is the overshoot during the resting phase, $\Delta\bar{\eta}_{peak}$ is the difference between the peak height of each motion law and the *optimal* trajectory, and $\Delta\bar{\eta}_{rest}$ represents the overshoot difference between the considered motion law and the optimal one during the resting phase. In the video supplied as supplementary material, the liquid motions corresponding to the trajectories compared in this experiment are captured.

In many practical applications such as automatic filling machines, the fill level of the container is usually not constant throughout its whole processing, and the implementation of different motion laws according to the fill level may be impractical. Therefore, it is interesting to test the robustness of the proposed trajectory planning with respect to such parameter. In this respect, we notice that the natural frequency ω_n in (3) of the sloshing model first increases sharply with the fill level h and

Table 1
Peak sloshing heights for different motion laws.

	$\bar{\eta}_{peak}$ mm	$\lvert\bar{\eta}_{rest,peak}\rvert$ mm	$\Delta\bar{\eta}_{peak}$ mm	$\Delta\bar{\eta}_{rest}$ mm
optimal	**7.525**	**0.875**	–	–
poly5	7.175	2.450	−0.350	1.575
trapezoidal	8.400	2.450	0.875	1.575
trapez. unconstrained	10.15	4.375	2.625	3.500

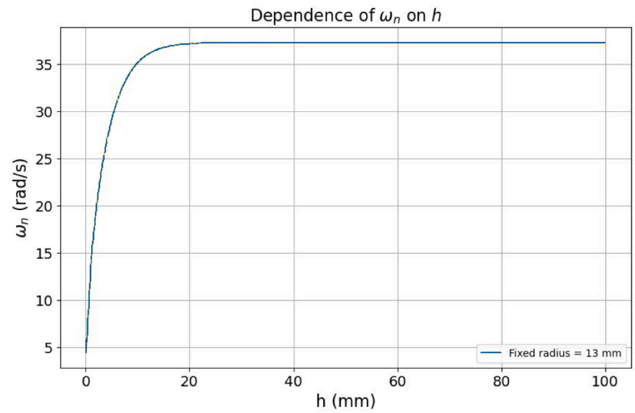

Fig. 9. Natural frequency ω_n vs. level h.

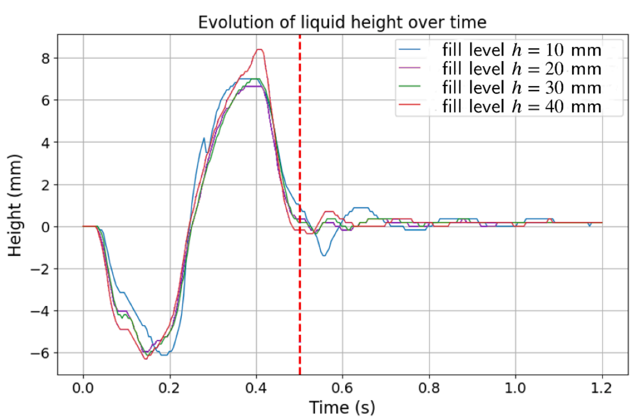

Fig. 10. Comparison of sloshing height by applying the optimized motion law to vials with different fill levels h.

then it saturates when the liquid height exceeds the bottle radius R (see Fig. 9).

This suggests that if the motion law is designed considering a fill height greater than the radius, it will remain reasonably valid for higher fill levels. Conversely, if the fill level falls below the radius, the liquid behavior may no longer be consistent. To experimentally validate this observation, the optimized motion law, computed for $R = 13$ mm and $h = 28$ mm, has been applied to containers with different fill levels, ranging from a height lower than the radius up to a near-maximum capacity. The evolution of the free surface height over time, shown in Fig. 10, supports the claim.

5. Conclusion

Within the context of automated packaging systems, a novel optimization-based motion planning methodology has been proposed in this paper, with the aim of mitigating the liquid sloshing phenomenon. As opposed to existing techniques, direct optimization of the trajectory is performed by solving a suitable constrained optimal control problem which ensures low while-in-motion and residual oscillations. The proposed method has been validated on a dedicated testbed and its performance has been compared to that of state-of-the-art methods, showing a significant improvement.

CRediT authorship contribution statement

Francesco Grassi: Conceptualization, Investigation, Methodology, Software, Validation, Writing – original draft; **Gianni Bianchini:** Conceptualization, Investigation, Methodology, Supervision, Writing – review & editing; **Simone Paoletti:** Conceptualization, Investigation, Methodology, Supervision, Writing – review & editing; **Tommaso Matassini:** Resources, Supervision, Validation, Writing – review & editing.

Declaration of competing interest

The authors declare the following financial interests/personal relationships which may be considered as potential competing interests:

Gianni Bianchini serves as associate editor for the European Journal of Control. Given his role, he had no involvement in the peer review of this article and had no access to information regarding its peer review. Full responsibility for the editorial process for this article was delegated to another journal editor. If there are other authors, they declare that they have no known competing financial interests or personal relationships that could have appeared to influence the work reported in this paper.

Supplementary material

Supplementary material associated with this article can be found in the online version at 10.1016/j.ejcon.2026.101613.

References

Alshaya, A., & Almujarrab, D. (2021). A smooth polynomial shaped command for sloshing suppression of a suspended liquid container. *Transactions of the Institute of Measurement and Control*, *43*(2), 278–294.

Aribowo, W., Yamashita, T., & Terashima, K. (2015). Integrated trajectory planning and sloshing suppression for three-dimensional motion of liquid container transfer robot arm. *Journal of Robotics*, *2015*, (pp. 279460–279474).

Biagiotti, L., & Melchiorri, C. (2008). Trajectory planning for automatic machines and robots. Springer.

Di Leva, R., Carricato, M., Gattringer, H., & Müller, A. (2021). Time-optimal trajectory planning for anti-sloshing 2-dimensional motions of an industrial robot. In *20th international conference on advanced robotics (ICAR 2021)* (pp. 32–37). Ljubljana, Slovenia.

Feddema, J., Dohrmann, C., Parker, G., Robinett, R., Romero, V., & Schmitt, D. (1997). Control for slosh-free motion of an open container. *IEEE Control Systems Magazine*, *17*(1), 29–36.

Grundelius, M. (2000). Iterative optimal control of liquid slosh in an industrial packaging machine. In *Proceedings of the 39th IEEE conference on decision and control* (pp. 3427–3432).

Grundelius, M., & Bernhardsson, B. (1999). Control of liquid slosh in and industrial packaging machine. In *Proceedings of the 1999 IEEE international conference on control applications* (pp. 1654–1659).

Guagliumi, L., Berti, A., Monti, E., & Carricato, M. (2021). A simple model-based method for sloshing estimation in liquid transfer in automatic machines. *IEEE Access*, *9*, 129347–129357.

Guagliumi, L., Berti, A., Monti, E., & Carricato, M. (2022). Antisloshing trajectories for high-acceleration motions in automatic machines. *Journal of Dynamic Systems, Measurement, and Control*, *144*(7), 071006.

BauerH. F. (1966). Nonlinear mechanical model for the description of propellant sloshing. *AIAA Journal*, *4*(9), 1662–1668.

Ibrahim, R. A. (2005). Liquid sloshing dynamics: Theory and applications. Cambridge University Press.

Khorshid, E., & Al-Fadhli, A. (2020). Optimal command shaping design for a liquid slosh suppression in overhead crane systems. *ASME Journal of Dynamic Systems, Measurement, and Control*, *143*(2), 021005.

Melchiorri, C., Biagiotti, L., Moriello, L., & Paoli, A. (2018). Manipulating liquids with robots: A sloshing-free solution. *Control Engineering Practice*, *78*, 129–141.

Noda, Y., Yano, K., Horihata, S., & Terashima, K. (2004). Sloshing suppression control during liquid container transfer involving dynamic tilting using wigner distribution analysis. In *43rd IEEE conference on decision and control (CDC)* (pp. 3045–3052).

Pridgen, B., Bai, K., & Singhose, W. (2010). Slosh suppression by robust input shaping. *Proceedings of the 49th IEEE conference on decision and control (CDC)*, (pp. 2316–2321).

Rawlings, J. B., Mayne, D. Q., & Diehl, M. M. (2022). Model predictive control: Theory, computation, and design. Nob Hill.

Richter, H. (2010). Motion control of a container with slosh: Constrained sliding mode approach. *ASME Journal of Dynamic Systems, Measurement, and Control*, *132*(3), 031002.

Yano, K., & Terashima, K. (2005). Sloshing suppression control of liquid transfer systems considering a 3-D transfer path. *IEEE/ASME Transactions on Mechatronics*, *10*(1), 8–16.